International Journal of Adhesion & Adhesives xxx (xxxx) xxx

Contents lists available at ScienceDirect

International Journal of Adhesion and Adhesives

journal homepage: http://www.elsevier.com/locate/ijadhadh

Pretreatment using diluted epoxy adhesive resin solution for improving bond strength between steel and wood surfaces

Bo Tan [a,b], Yi Ji [b], Yunsen Hu [b], Bingyan Yuan [b], Xiaozhi Hu [b,*], Zhaohui Huang [a]

[a] School of Materials Science and Technology, Beijing Key Laboratory of Materials Utilization of Nonmetallic Minerals and Solid Wastes, National Laboratory of Mineral Materials, China University of Geosciences, Beijing, 100083, PR China
[b] Department of Mechanical Engineering, University of Western Australia, Perth, WA, 6009, Australia

ARTICLE INFO

Keywords:
Laminar composites
Jarrah wood
Resin pre-coating (RPC)
Intralaminar failure

ABSTRACT

Interfacial bonding strength is critical to key structural functions in the laminar composite of different substrates bonded together by adhesives. This paper reports a study on utilization of the micro-porous composite structures of a hard-Australian jarrah wood to enhance the adhesive bonding with steel substrates. The thin adhesive joint between the two different substrates is rooted deeply into the micro-channels within the micro-porous composite structures of the jarrah wood using a unique resin pre-coating (RPC) technique. The mechanical abrasion of the substrates was carried out before RPC. Based on single lap shear tests, over 180% of improvement in shear strength was achieved after optimizing the concentration of RPC solution. One important observation was the wettability of substrates was enhanced by RPC as well. A non-destructive technique, X-ray tomography, was employed to reveal the microstructural details of jarrah wood, confirming the usefulness and effectiveness of RPC.

1. Introduction

Due to high specific stiffness and strength, various laminar composites such as carbon fiber reinforced polymer (CFRP), lightweight core and wood sandwich structure materials, have been increasingly used in a wide range of engineering applications of aircraft, marine and high-speed railways [1]. Among all the basic material, wood is an ideal core material for composites, due to the high strength/weight ratio, easy fabrication and relatively low cost [2,3]. Epoxy adhesives are mainly used for the interfacial bonding of those laminar composites, forming stable layered structures without any mechanical fasteners and bolts [4,5]. With increasing demand for light-weight composites in high-performance structures, hybrid joints between wood and other materials such as metal [6], glass [7] and plastic [8] have drawn much wider attention in industries. Among all the potential industrial applications, interfacial bond strength has to be the key for the structural performance of those laminar composites considering the property variation across the interface and the consequent stress concentration [9].

Within an adhesive joint in a laminar composite structure, adhesive bonding is linked to the adhesive strength (cohesive strength within the adhesive) and the interfacial strength between the substrate and adhesive, and to some extent the mechanical interlocking of the polymer adhesive with the substrate [10]. Depending on the crack location and crack growth path, distinct failure modes can be defined as following four failure modes [11], i.e. (i) Adhesion failures occur at the interface between the adhesive and one of the substrates, or cracking along the bonding interface; (ii) Cohesion failures result in cracking within the adhesive; (iii) Mixed-mode failures are common, exhibiting characteristics of both adhesion and cohesion failures; (iv) Intralaminar failure in a micro-porous composite substrate, can happen when the strength of the internal structure of the substrate is lower than that of the interfacial adhesive bond. This composite structure failure will be the focus of this study.

In this paper, we focus on the adhesive bonding between wood and metal substrates with big difference in hardness and structure in terms of micro-porosity. As the most common metal material, steel has wide applications in construction industries [12], rail engineering [13], and aircraft manufacture [14]. As one unique hardwood from the southwest of Western Australia, jarrah wood has excellent properties, such as high corrosion resistance, waterproofness and high hardness making it one of the most popular timbers in the application of construction and decoration in Australia [15].

Fig. 1 shows the 3D images of the internal structures of jarrah wood

* Corresponding author.
E-mail address: xiao.zhi.hu@uwa.edu.au (X. Hu).

https://doi.org/10.1016/j.ijadhadh.2019.102502

Available online 9 November 2019

revealed by X-ray tomography. Jarrah like any wood is an anisotropic and porous composite material with many anatomical features. Major elements of the jarrah structures are longitudinal tracheids and fibers and vessel elements. The lumens of these cells and interconnecting pits provide an excellent pathway for liquid-phase resin flow and diffusion for potential stronger adhesive bonding. However, high molecular weight and sticky resins, or occlusions in the pits or lumens, and limited micro-openings in the wood microstructures may prevent deep resin penetration. Therefore, a unique resin pre-coating (RPC) technique [16] is adopted in this study to promote a deep resin penetration into the wood composite structures. The RPC solution contains 10–30 wt% epoxy resin (without hardener) with 70–90 wt% acetone. Considering the environmental influence from organic solvent, using an aqueous system will be part of further work.

RPC is also an effective method to enhance the wettability of substrates and reduce the sub-surface micro-voids in the bonding area, according to the previous studies on epoxy adhesion bonding between substrates of steel-steel [17] and CFRP-metal [18,19]. As displayed in Fig. 2, a rough wood surface contains many micro-voids and micro-cavities either from surface polishing/sanding or metaxylem vessels. When an adhesive resin is applied directly, the resin flow can be impeded due to the poor wettability of a wood substrate; particularly the subsurface micro-voids cannot be effectively penetrated by an epoxy adhesive. An RPC solution containing 10–30 wt% resin (with no hardener) can effectively penetrate into all subsurface micro-voids and wet the substrate surface. After evaporation of acetone, the wood-substrate remains coated by an ultra-thin layer of resin, and all subsurface micro-voids are filled. With the improved substrate wettability, the normal epoxy adhesive (resin with hardener) can be applied. The cross-linking process or diffusion of hardener can gradually move deeply into those subsurface micro-voids filled by resin applied with the RPC process. As a result, the epoxy resin from RPC in the subsurface micro-voids will be cured, and the epoxy adhesive joint can be deeply rooted into the micro-porous composite structures of jarrah wood, leading to much improved interfacial bond strength.

2. Experiment details

2.1. Materials

In this study, commercially available jarrah wood bars of dimension 1000 mm × 25 mm × 8 mm purchased from Graham's Joinery (Perth, Western Australia) were selected as wood substrate. Flat steel bars of dimension 6000 mm × 25 mm × 3 mm purchased from Midalia Steel (Perth, Australia) were used as steel substrate. They were cut into small pieces of size 80 mm × 25 mm and shim pieces of size 25 mm × 25 mm. The SELLEYS Araldite Super Strength Epoxy Adhesive composed of resin and hardener was purchased from Bunnings Warehouse (Perth, Australia) as the adhesive. Only the resin (but not also the hardener) was used for RPC. Acetone was used to clean the surface of steel substrates and prepare the RPC solution. The FT-IR analysis of resin can be found in the supplementary information. 120 # SiO_2 sandpapers from Bunnings Warehouse (Perth, Australia) were used for polishing the jarrah substrates. Grit blasting for the steel substrates was carried out by GMA Premium Blast machine assisted by UWA Engineering Faculty Workshop (Perth, Australia).

2.2. Surface cleaning and mechanical abrasion

First, all the steel substrates were ultrasound cleaned in acetone solution at room temperature for 45 min to remove any dust and possible oil contamination. Next, the cleaned steel substrates were grit blasted under the following constant condition: Garnet grits in size of 30–60 μm, applied at the compressed air of 5 bars in distance of 100 mm for 10 s per sample. Then the steel substrates were cleaned in acetone again for 45 min, assisted by ultrasound. After drying, the roughened steel substrates were ready for adhesive bonding.

All the jarrah substrates were cleaned by compressed air to remove dust from the surface. Then, the jarrah wood substrates were polished for 10 s by 120 # SiO_2 sandpaper, followed by again surface cleaning assisted by compressed air. After those simple surface preparations, the roughened jarrah wood substrate samples were ready for adhesive bonding.

The macro photographs and SEM images of steel and jarrah wood substrates after mechanical abrasion were shown in Fig. 3. The grit blasting method removed all the oxide layer on the steel surface, and produced bumps and hollows, as illustrated by Fig. 3a. For jarrah substrates, sandpaper produced many cracks and pits on the substrate surface as displayed in Fig. 3b. It indicates that the mechanical abrasion lead to a significant enhancement in surface roughness.

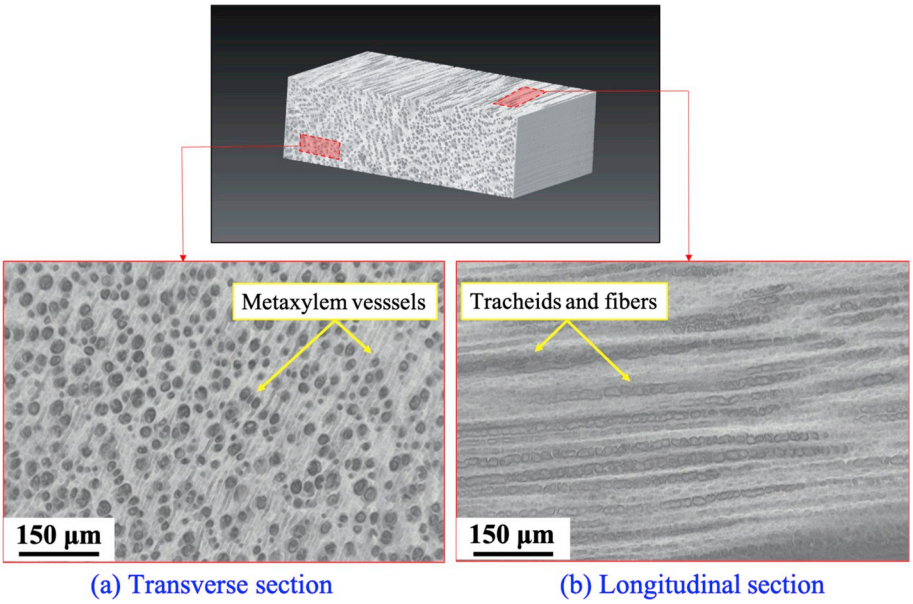

Fig. 1. Microscopic Metaxylem structures of jarrah wood substrate revealed by X-ray tomography.

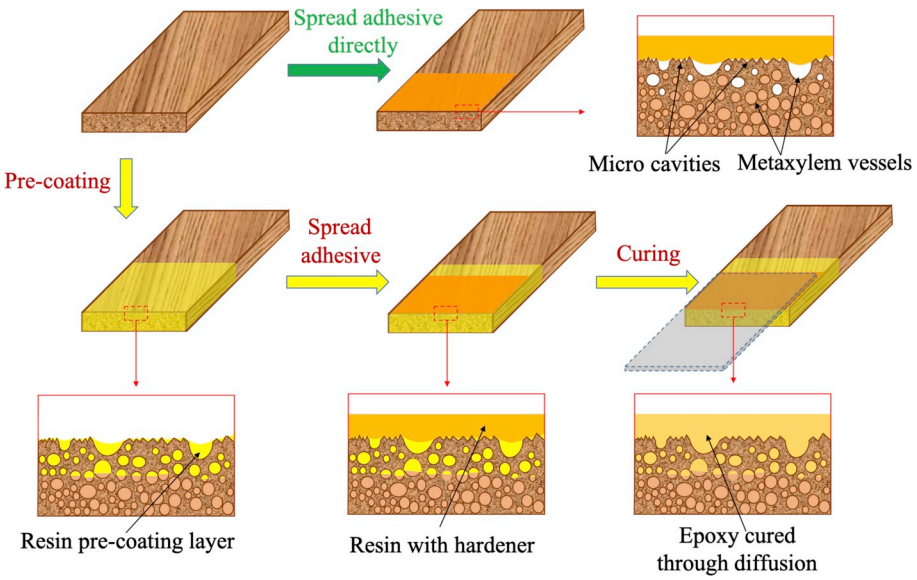

Fig. 2. Sealing of subsurface micro-voids in composite wood substrate using resin pre-coating (RPC).

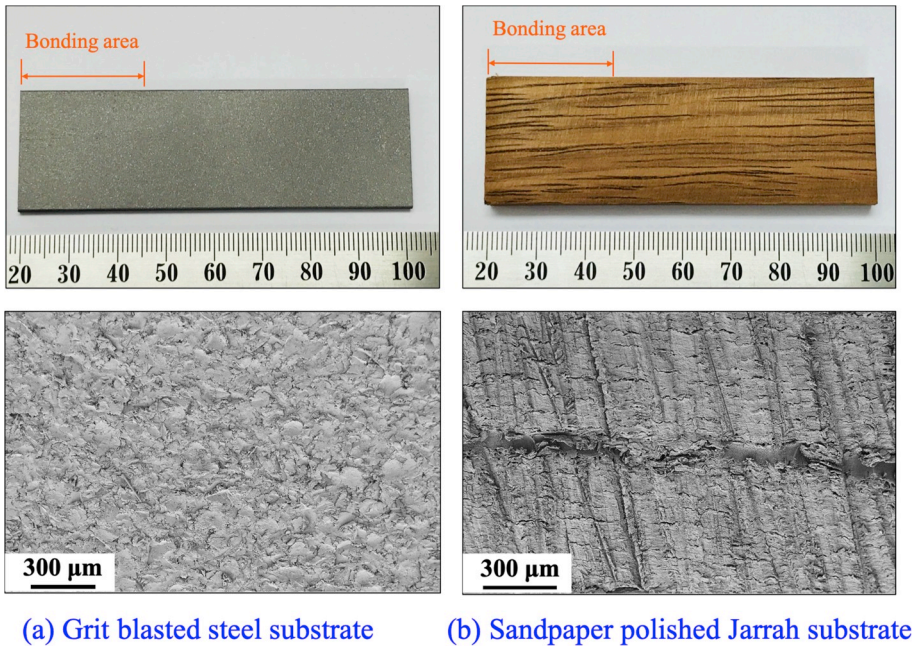

Fig. 3. Macro photographs and SEM images of (a) grit blasted steel substrate, (b) 120# SiO_2 sandpaper polished jarrah wood substrate.

2.3. RPC treatment

The solutions for the RPC treatment were prepared by dissolving the epoxy resin (without hardener) in acetone. According to a previous study [16], 10 wt% of epoxy resin-acetone solution was chosen for steel substrates RPC treatment. Three kinds of resin-acetone solution with different concentrations of 10 wt%, 20 wt%, and 30 wt% were set for the jarrah wood substrates. The RPC treatment was applied by dipping the substrates into the resin-acetone solution for 10 s and dried in a fuming cupboard at room temperature for 30 min to let acetone completely evaporating. The sample surface with RPC is shown in Fig. 5a and b, where the pre-coated area appears to be a little darker.

SEM photos on microscopic details of the pre-coated steel and jarrah wood substrates were shown in Fig. 4c–f. It was clear that resin from RPC had penetrated into the microcavities and fissures on steel and jarrah substrates surface. Remaining resin filled the pits on the steel substrates in Fig. 4c. The photos showed an increase in the residual amount of resin on the surface of pre-coated jarrah substrates from 10 wt% to 30 wt% concentration of the solution, as schematically illustrated in Fig. 4d, e, and f. The effectiveness of RPC was proven by surface roughness analysis. All substrates showed the same features as expected from RPC.

2.4. Preparation of standard testing samples

The shear strength of those steel-jarrah composite samples was measured by the Single Lap Shear (SLS) test method. According to ASTM D 2339–98 (2004), the bonding area was determined to be 25 mm × 25 mm. The final samples geometry and dimension were illustrated in Fig. 5.

Five specimens with different surface conditions were studied, i.e. (i) Control, assembled by as-received steel and jarrah substrates; (ii) G120, made by grit blasted steel substrates and jarrah substrates polished by

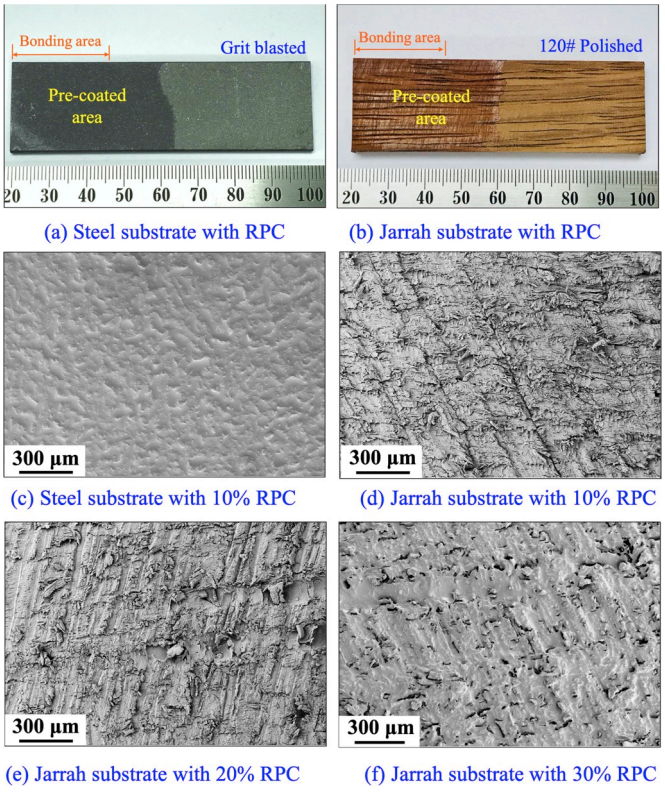

Fig. 4. Macro photographs of pre-coated (a) steel substrates and (b) jarrah substrates, corresponding SEM images of pre-coated (c) steel substrates and (d–f) jarrah substrates with different RPC solution concentration (10–30 wt%).

120# sandpaper; (iii - v) P10, P20, and P30, assembled by grit blasted steel substrates pre-coated by 10 wt% of resin-acetone solution and 120# sandpaper polished jarrah substrates pre-coated by 10 wt%, 20 wt %, and 30 wt% of resin-acetone solution respectively. The surface treatment details of substrates in each testing specimen were listed in Table 1.

To achieve constant adhesive thickness and bond area among all specimens, glued samples were pressed down by small spring clamps. During the curing process, the samples were kept in an oven for 20 min at 40 °C for initial shape setting firstly, followed by 60 °C for 10 h for complete curing.

2.5. Analytical and mechanical test methods

The interior structure of jarrah wood was observed via X-ray tomography by a Zeiss Versa 3D X-ray microscopy with sub-micron resolution (around 700 nm minimum). The microstructures of substrates surface and sheared adhesive bonding joints were observed by the scanning electron microscopy (SEM). The surface roughness was

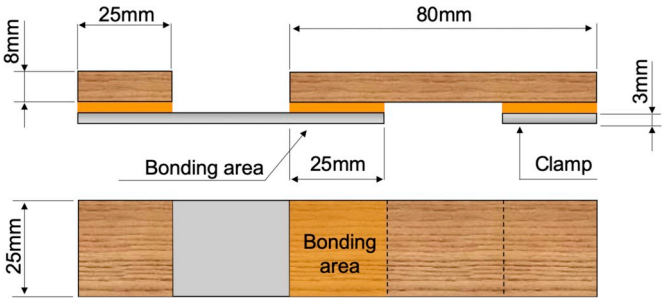

Fig. 5. SLS testing specimen dimensions.

Table 1
Surface treatment details of substrates in SLS testing specimens.

Samples	Steel substrates		Jarrah substrates	
	Grit blasting	RPC	Sandpaper Polishing	RPC
Control	–	–	–	–
G120	Done	–	Done	–
P10	Done	10 wt%	Done	10 wt%
P20	Done	10 wt%	Done	20 wt%
P30	Done	10 wt%	Done	30 wt%

determined by a profilometer (Altisurf 520, ALTIMET) with a travel distance of 10 mm × 10 mm. Contact angle measurement was carried out to investigate the wettability of substrates after surface treatment. The tensile shear strength was measured by the SLS tests using an Instron 5982 mechanical testing machine with a 100 KN load range. The tests were carried out under a constant displacement rate of 1 mm/min. Six samples had been tested for each type of bonding.

3. Results and discussion

3.1. Influence of the RPC method on the wettability between adhesive and substrates

The surface wettability between adhesive and substrate is critical in the epoxy composite system for achieving high adhesive surface coverage and final bonding strength. The influence of the RPC method on wettability was investigated for six different surface conditions by contact angle test. They are (1) grit blasted steel surface; (2) grit blasted steel surface with 10 wt% RPC; (3) sandpaper polished jarrah surface; (4–6) sandpaper polished jarrah surface with 10 wt%, 20 wt% and 30 wt % of RPC treatment respectively.

A drop of well-mixed two-part epoxy (epoxy resin & hardener) of about 0.1 ml was dropped onto the six testing surfaces at room temperature by a dropper. The spreading process and contact angle of these drops on the substrates were recorded by the Dino Lite microscope after 5s, 30s and 60s respectively. The contact angle for the various substrates surface conditions are listed in Table 2. The typical spreading extent was shown in Fig. 6. The development of the contact angle on jarrah substrates can also be seen from Fig. 7. The RPC treatment improved the wettability, seen as lower contact angles and higher spreading speed. The concentration of the RPC solution, however, showed only small influence on the wettability. It appeared that the wettability of the rough substrates (both steel and jarrah wood substrates) have been improved by the RPC treatment. It maybe because the roughened surface somehow limited movement of the thick epoxy mixture [16]. When RPC technique was adopted, remaining resin filled the pits and covered the rough surface of the jarrah substrates. Due to the remaining epoxy layer with similar adhesive component on the substrates surface from the RPC, better wettability achieved.

3.2. The effects of RPC method on bonding strength

The measured shear strengths are listed in Table 3 and shown in Fig. 8a; minimum and maximum shear strengths belong to each individual specimen category. An obvious improvement in bonding strength has been achieved by applying the RPC methods. Compared with G120, all the samples treated by the RPC method gave a significant enhancement in shear strength. P20 had the highest shear strength (12.3 MPa), showing 40% improvement compared to 8.8 MPa of G120, and had the minimum standard deviation as well. Moreover, even the minimum shear strength within the P20 category was higher than the maximum value within the G120 group. P10 and P30 displayed similar average shear strengths of 10.3 MPa and 10.0 MPa, respectively. In contrast with the Control, the increase in shear strength of P10, P20, and P30 achieved 134%, 180%, and 127%, respectively.

Table 2
Results of contact angles testing.

Steel (Grit blasted)	Time (s)	Contact Angle (deg.)		Jarrah (Polished)	Time (s)	Contact Angle (deg.)			
		Without RPC	10 wt% RPC			Without RPC	10 wt% RPC	20 wt% RPC	30 wt% RPC
	5	52.5	44.8		5	45.6	42.2	40.3	41.3
	30	42.2	25.8		30	38.5	31.7	30.4	31.7
	60	38.4	20.9		60	34.3	25.9	23.7	25.7

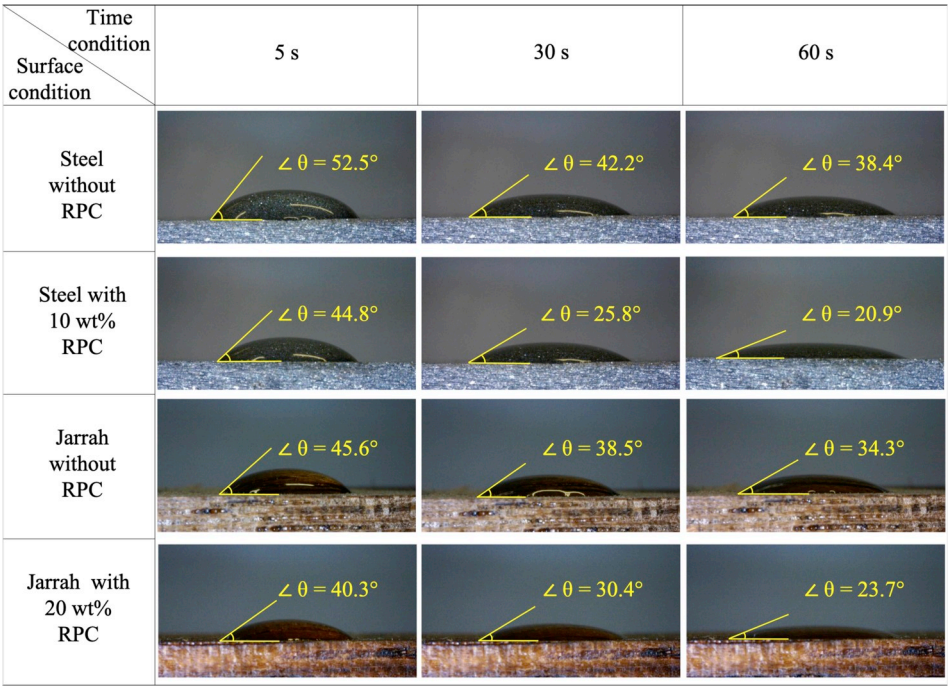

Fig. 6. Cross section view of contact angle measurements for steel and jarrah wood substrates surface.

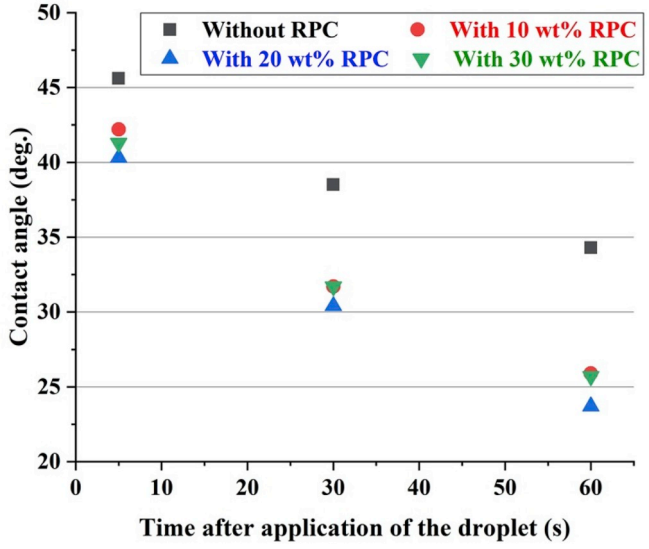

Fig. 7. Change of the contact angle on jarrah substrates.

The loading energies are displayed in Fig. 8b, the typical loading-displacement curves are shown in Fig. 8c. The shear failure process can be divided into three stages: (I) the initial elastic region associated with elastic deformation of the epoxy adhesive; (II) the non-linear region associated with epoxy plastic deformation and interface debonding; (III) another region with nearly linear increase and partly already with occurring epoxy cohesive failure and structure failure. The increasing peak loads increasing were mainly due to the elongated region of (III) for samples [20]. With this also loading energy as the area underneath the load-displacement curves increased.

3.3. Failure patterns observation and reinforcement mechanisms analysis

Fig. 9 displays the sheared surfaces of the test samples. A large area of oxide layer debonding was found on the sheared surface of Control as shown in Fig. 9a. Due to the weak and porous oxide layer, adhesion was separated within the steel substrates. Therefore the loading curve of the Control samples stopped at stage (II) as shown in Fig. 8c, associated with oxide layer debonding. Adhesive failure occurred predominantly for G120 (sample without RPC) in Fig. 9b, in combination with smaller extent of structural wood failure. As displayed in Fig. 10a and b, lots of empty pits and pores appeared on the microstructure of typical adhesive failure area, which indicated that the adhesive did not fill into those micro-pits so that defects were formed. A noticeable intralaminar failure area along the surface of the substrate can be observed in the cases of RPC treatment, as shown in Fig. 9c–e. Especially in the case of P20 complete intralaminar failure (wood failure) occurred. P10 showed both, structural wood failure and, to a lesser extent, cohesive adhesive failure.

For the cohesive failure area on P10, as shown in Fig. 10c and d, it is hard to see any pores on the microstructure. Besides, it contains many interlocked epoxy sites embedded in the substrates. The epoxy interlocking mechanism for higher shear strength is only possible when resin can fully penetrate deep into the microcavities and fissures, created by grit blasting, which showed the benefit of the RPC method. For the

Table 3
Shear strengths.

Specimen category	RPC condition (wt%)		Average Shear strength (MPa)	Maximum Shear strength (MPa)	Minimum Shear strength (MPa)	Standard deviation (MPa)
	Steel	Jarrah				
Control	-	-	4.4	5.7	2.9	1.2
G120	-	-	8.8	10.1	7.4	1.1
P10	10	10	10.3	12.2	8.0	1.4
P20	10	20	12.3	12.7	11.5	0.4
P30	10	30	10.0	11.8	8.4	1.3

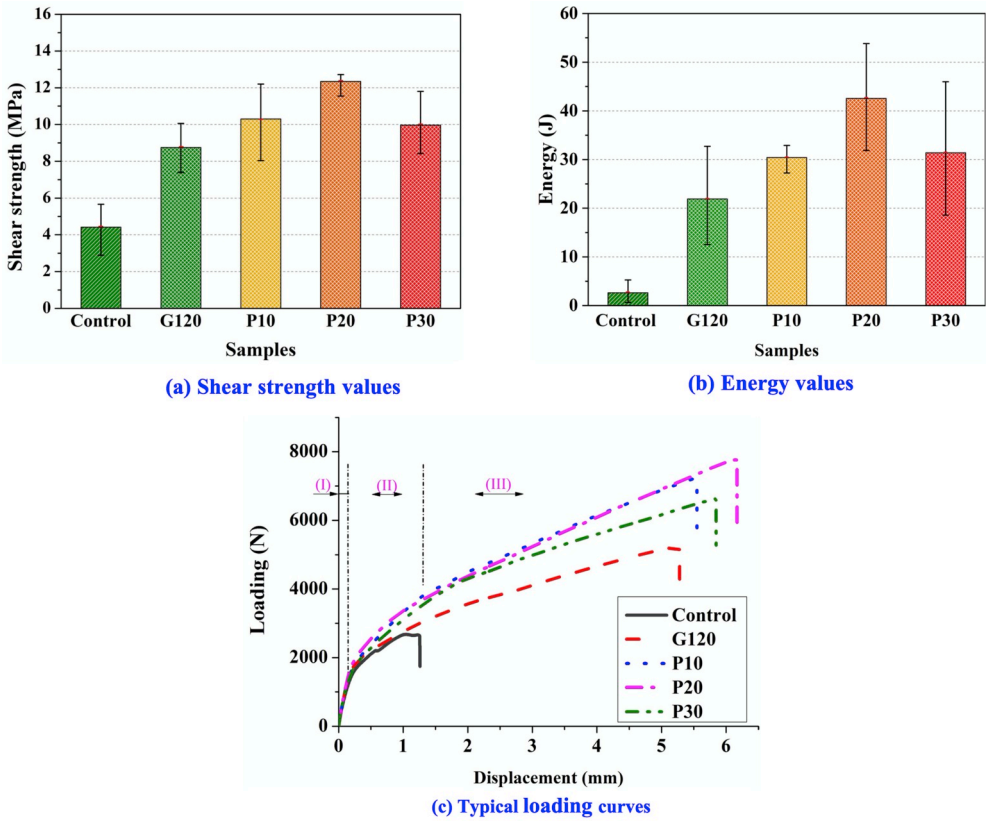

Fig. 8. Diagrams of (a) shear strengths, (b) loading energy values and (c) typical load-displacement curves for adhesive bonding samples by SLS testing.

intralaminar failure area, many wood fibers breaking can be found in this area as in Fig. 10e and f. It indicates that the acetone has taken resin into the internal surface structure of jarrah substrates and reinforced this bonding area interphase. The thin adhesive joint between the substrates is rooted deeply into the micro-channels within the micro-porous jarrah wood substrate and produced high bonding strength.

Among the samples prepared with RPC, the shear strength of P30 is lower than that of P20, this indicates that the resin concentration in the RPC solution should not be too high, as the hardener in the two-component epoxy adhesive added after the RPC process may not be sufficient for diffusion and curing of the RPC region with such a large amount of resin present there. On the other side, also the P10 showed lower shear strength and only mixed failure mode compared to full wood failure of P20; the behaviour of P10 points to a possibly too weak RPC effect due to the restricted amount of resin in the low concentration solution. Therefore, the 20 wt% would be the most appropriate RPC solution concentration for jarrah wood substrates.

In a way, the thin adhesive joint between the two different substrates was rooted deeply into the micro-channels within the jarrah wood by the RPC technique. Thus the failure mode of the jarrah-steel epoxy joint was improved from adhesive failure (G120, Fig. 9b) along the steel/jarrah interface into mixed modes of jarrah structural wood failure and cohesive adhesive fracture (P10, Fig. 9c), and even the whole intralaminar wood failure (P20, Fig. 9d) so that the maximum reinforcing effect was achieved.

4. Conclusions

This paper has examined various interfacial failure modes of an adhesive joint between a micro-porous wood composite substrate and a solid metal substrate. A special resin pre-coating (RPC) technique has been adopted to promote deep penetration of an epoxy adhesive into the subsurface micro-voids in the micro-porous wood material, leading to substantial improvement in the adhesive bond strength. The RPC method also improved the wettability between adhesive and substrates.

Based on the shear strength tests, 20 wt% of resin in acetone was proven to be the most effective RPC solution for jarrah wood. The corresponding sample P20 (sample assembled by grit blasted steel substrate with 10 wt% of RPC solution and 120 # sandpaper polished jarrah wood substrates with 20 wt% of RPC solution) yielded the best testing results among all specimens with an improvement of 180% in comparison to the Control. Surface topography and Scanning Electron Microscope (SEM) observations showed that RPC improved the failure mode of jarrah-steel epoxy joint from cohesive failure within the oxide layer of

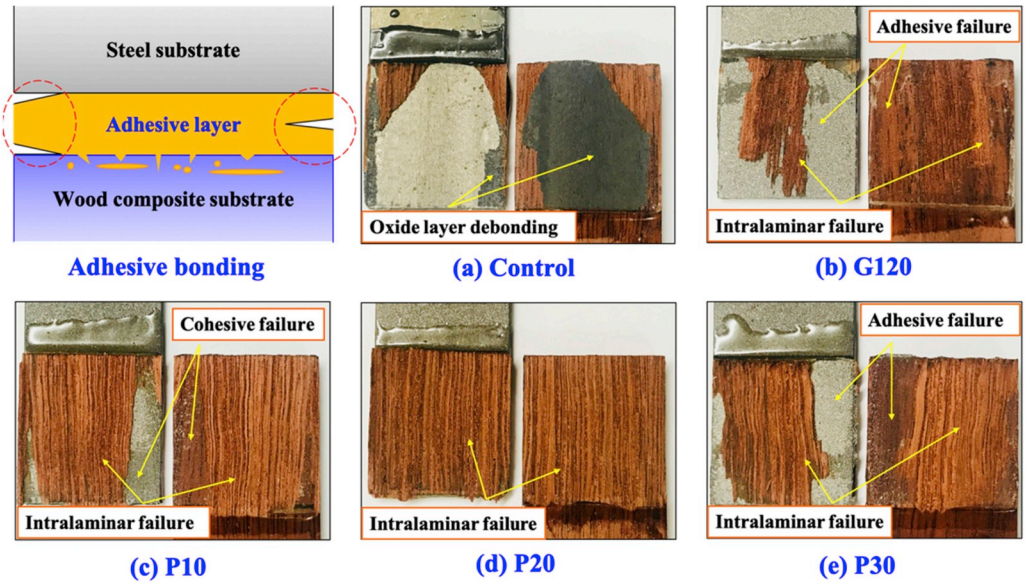

Fig. 9. Schematic of adhesive bonding and shear failure interface images of (a) Control, as-received sample; (b) G120, substrates without RPC; (c) P10, jarrah substrates with 10 wt% RPC; (d) P20, jarrah substrates with 20 wt% RPC; (e) P30, jarrah substrates with 30 wt% RPC.

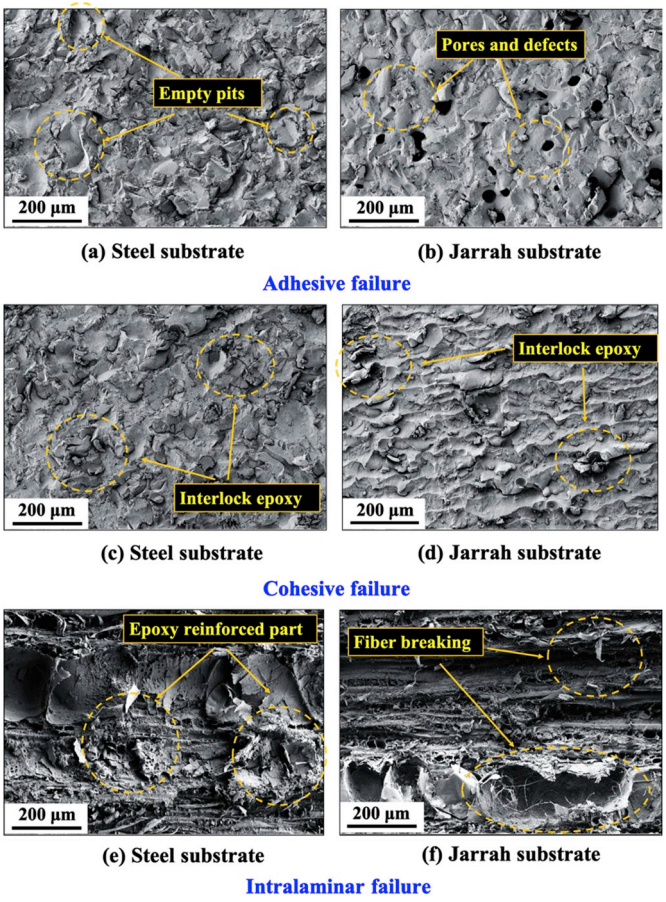

Fig. 10. SEM images of typical failure mode on sheared steel and jarrah wood substrates surface.

the steel substrates to mixed modes of jarrah wood failure and fracture along the jarrah and steel interphase and even to whole wood failure of jarrah.

Acknowledgements

Financial support from the China Scholarship Council (201606400039), technical supports of X-ray tomography and SEM analysis from the UWA Centre of Microscopy, Characterization and Analysis and assistance in sample preparation from UWA Engineering Faculty Workshop are gratefully acknowledged.

Appendix A. Supplementary data

Supplementary data to this article can be found online at https://doi.org/10.1016/j.ijadhadh.2019.102502.

References

[1] Zhang K, Yang Z, Li Y. A method for predicting the curing residual stress for CFRP/Al adhesive single-lap joints. Int J Adhesion Adhes 2013;46:7–13. https://doi.org/10.1016/j.ijadhadh.2013.05.010.
[2] Rescalvo FJ, Aguilar-Aguilera A, Suarez E, Valverde-Palacios I, Gallego A. Acoustic emission during wood-CFRP adhesion tests. Int J Adhesion Adhes 2018;87:79–90. https://doi.org/10.1016/j.ijadhadh.2018.09.007.
[3] Shi H, Liu W, Fang H, Bai Y, Hui D. Flexural responses and pseudo-ductile performance of lattice-web reinforced GFRP-wood sandwich beams. Compos B Eng 2017;108:364–76. https://doi.org/10.1016/j.compositesb.2016.10.009.
[4] Duan K, Hu X, Mai Y-W. Substrate constraint and adhesive thickness effects on fracture toughness of adhesive joints. J Adhes Sci Technol 2004;18(1):39–53. https://doi.org/10.1163/156856104322746992.
[5] Custódio J, Broughton J, Cruz H. A review of factors influencing the durability of structural bonded timber joints. Int J Adhesion Adhes 2009;29(2):173–85. https://doi.org/10.1016/j.ijadhadh.2008.03.002.
[6] Yeboah D, Taylor S, McPolin D, Gilfillan R, Gilbert S. Behaviour of joints with bonded-in steel bars loaded parallel to the grain of timber elements. Constr Build Mater 2011;25(5):2312–7. https://doi.org/10.1016/j.conbuildmat.2010.11.026.
[7] Blyberg L, Serrano E, Enquist B, Sterley M. Adhesive joints for structural timber/glass applications: experimental testing and evaluation methods. Int J Adhesion Adhes 2012;35:76–87. https://doi.org/10.1016/j.ijadhadh.2012.02.008.
[8] Cui Y, Lee S, Noruziaan B, Cheung M, Tao J. Fabrication and interfacial modification of wood/recycled plastic composite materials. Compos Part A Appl Sci Manuf 2008;39(4):655–61. https://doi.org/10.1016/j.compositesa.2007.10.017.
[9] Bai L, Li Z, Zhao S, Zheng J. Covalent functionalization of carbon nanotubes with hydroxyl-terminated polydimethylsiloxane to enhance filler dispersion, interfacial adhesion and performance of poly(methylphenylsiloxane) composites. Compos Sci Technol 2018;165:274–81. https://doi.org/10.1016/j.compscitech.2018.07.006.
[10] Wong DWY, Zhang H, Bilotti E, Peijs T. Interlaminar toughening of woven fabric carbon/epoxy composite laminates using hybrid aramid/phenoxy interleaves. Compos Part A Appl Sci Manuf 2017;101:151–9. https://doi.org/10.1016/j.compositesa.2017.06.001.

[11] Brandtner-Hafner M. Interface fracture mechanics of notched wood-adhesive composites and mode I, II, III loading. In: Int symp notch fract, vol. 04; 2017. p. 29–31. https://www.researchgate.net/publication/315833570.
[12] Grujicic M, Sellappan V, Kotrika S, Arakere G, Obieglo A, Erdmann M, Holzleitner J. Suitability analysis of a polymer–metal hybrid technology based on high-strength steels and direct polymer-to-metal adhesion for use in load-bearing automotive body-in-white applications. J Mater Process Technol 2009;209(4): 1877–90. https://doi.org/10.1016/j.jmatprotec.2008.04.050.
[13] Nicoli E, Dillard DA, Dillard JG, Campbell J, Davis DD, Akhtar M. Using standard adhesion tests to characterize performance of material system options for insulated rail joints. P I Mech Eng F-J Rai 2011;225(5):509–22. https://doi.org/10.1177/2041301710392481.
[14] Vietri U, Guadagno L, Raimondo M, Vertuccio L, Lafdi K. Nanofilled epoxy adhesive for structural aeronautic materials. Compos B Eng 2014;61:73–83. https://doi.org/10.1016/j.compositesb.2014.01.032.
[15] Belfas J, Groves KW, Evans PD. Bonding surface-modified Karri and Jarrah with resorcinol formaldehyde. Holz Roh Werkst 1993;51:253–9. https://doi.org/10.1007/BF02629370.
[16] Wang B, Bai Y, Hu X, Lu P. Enhanced epoxy adhesion between steel plates by surface treatment and CNT/short-fibre reinforcement. Compos Sci Technol 2016; 127:149–57. https://doi.org/10.1016/j.compscitech.2016.03.008.
[17] Wang B, Hu X, Lu P. Improvement of adhesive bonding of grit-blasted steel substrates by using diluted resin as a primer. Int J Adhesion Adhes 2017;73:92–9. https://doi.org/10.1016/j.ijadhadh.2016.11.012.
[18] Sun Z, Shi S, Hu X, Guo X, Chen J, Chen H. Short-aramid-fiber toughening of epoxy adhesive joint between carbon fiber composites and metal substrates with different surface morphology. Compos B Eng 2015;77:38–45. https://doi.org/10.1016/j.compositesb.2015.03.010.
[19] Hu Y, Yuan B, Cheng F, Hu X. NaOH etching and resin pre-coating treatments for stronger adhesive bonding between CFRP and aluminium alloy. Compos B Eng 2019;178(107478). https://doi.org/10.1016/j.compositesb.2019.107478.
[20] He P, Chen K, Yu B, Yue CY, Yang J. Surface microstructures and epoxy bonded shear strength of Ti_6Al_4V alloy anodized at various temperatures. Compos Sci Technol 2013;82(82):15–22. https://doi.org/10.1016/j.compscitech.2013.04.007.